

Tropical Convection and the Energy Balance at the Top of the Atmosphere

DENNIS L. HARTMANN, LESLIE A. MOY, AND QIANG FU

Department of Atmospheric Sciences, University of Washington, Seattle, Washington

(Manuscript received 19 December 2000, in final form 30 April 2001)

ABSTRACT

Earth Radiation Budget Experiment (ERBE) and International Satellite Cloud Climatology Project (ISCCP) data are used in conjunction with a radiative transfer model to estimate the effect of various cloud types on the top-of-atmosphere radiation budget in convective regions of the Tropics. This analysis shows that individual convective cloud elements can have strongly positive or negative effects on the radiation balance. Nonetheless, the ensemble of cloud types that occurs in association with deep convection in the Tropics arranges itself so that the individual positive and negative contributions cancel each other when averaged over the convective cloud system. This behavior of the cloud ensemble is extremely interesting, and the authors speculate that it is indicative of feedbacks in the climate system that have not been explored adequately. A simple model is introduced that includes feedbacks that drive the net radiation in convective regions toward the net radiation in adjacent nonconvective areas. If the nonconvective regions have small cloud forcing, then this model predicts small net radiative forcing by the convective cloud ensemble. This feedback process requires that the circulations in the Tropics be sensitive to small SST gradients and that the convective cloud albedo be sensitive to the vertical motion.

1. Introduction

Among the interesting results of the Earth Radiation Budget Experiment (ERBE) were estimates of top-of-atmosphere cloud radiative forcing indicating a remarkable equality between strong reductions in outgoing longwave radiation (OLR) and strong reductions in absorbed solar radiation associated with tropical cloud systems. Each of these radiative forcings is on the order of 100 W m^{-2} , but they are of opposite sign and so their effects on the planetary energy budget strongly cancel (Ramanathan et al. 1989; Harrison et al. 1990). Similar top-of-atmosphere cancellation can be obtained by regressing ERBE data onto International Satellite Cloud Climatology Project (ISCCP) data (Hartmann et al. 1992; Ockert-Bell and Hartmann 1992), or by calculating the radiation balance directly from ISCCP data (Chou 1994; Rossow and Zhang 1995; Zhang et al. 1995; Chen et al. 2000). The effect of tropical convective clouds on the earth's top-of-atmosphere energy budget is small, but they tend to cool the surface and heat the atmosphere. The shortwave effect is felt mostly at the surface, and the longwave effect is felt mostly in the atmosphere (e.g., Collins et al. 1996).

Kiehl (1994) has argued that the cancellation of the longwave and shortwave cloud forcing at the top of the

atmosphere is essentially a coincidence arising from the temperature of the tropopause and the albedo of optically thick ice clouds. In his analysis Kiehl considers only one cloud type that has an albedo of 0.6. If the clear-sky albedo is 0.1, the shortwave cloud forcing for such a cloud in the Tropics is about 200 W m^{-2} . The clear-sky longwave flux for the Tropics is about 290 W m^{-2} . Therefore if the longwave cloud forcing is to be the 200 W m^{-2} required to balance the shortwave cloud forcing, then the cloud emission should be about 90 W m^{-2} . This corresponds to a blackbody temperature of about 200 K, which is approximately the temperature of the tropical tropopause. This simple calculation shows two things. First, it is possible for a tropical convective cloud system with typical observed properties to have equal longwave and shortwave cloud forcings. Second, these cloud forcings are large when the cloud covers 100% of the region of interest. If the cloud-top temperature or cloud albedo vary only a little, therefore, very large net cloud radiative forcings will be produced. Reducing the cloud albedo to 0.4 or moving the cloud top to 235 K (10 km) would give cloud forcings of $\pm 80 \text{ W m}^{-2}$, respectively, representing a cloud forcing equal in magnitude to the net radiative energy input to the Tropics. It is important to ask why tropical convective cloud systems do not produce large net radiative forcings.

Studies of tropical cloud convective complexes using geosynchronous satellite, aircraft, and radar data all suggest a wide dispersion in the altitude and structure of

Corresponding author address: Dennis L. Hartmann, Dept. of Atmospheric Sciences, University of Washington, Box 351640, Seattle, WA 98195-1640.
E-mail: dennis@atmos.washington.edu

clouds within these systems (e.g., Chen et al. 1996; Johnson et al. 1999). As we will illustrate here, ISCCP data suggest a wide range of optical depths for tropical convective clouds with tops in the upper troposphere, ranging from thick anvil clouds near the convective cores to thin cirrus near the edges of the anvil cloud. We believe it is important to ask why the ensemble of cloud optical properties gives a neutral net radiative forcing, when individual elements within the cloud system show such a wide range of net radiative forcings. Why does the ensemble of cloud types produce an average net radiation change near zero, when individual cloud types produce cloud radiative forcings of $\pm 100 \text{ W m}^{-2}$?

In this study we take data from a region in the Tropics with persistent deep convective clouds that shows a strong cancellation between the longwave and shortwave effects of the cloud. We first show that we can approximate the ERBE observations of broadband radiative fluxes using ISCCP cloud data, observed atmospheric humidity and temperature profiles, and a radiative transfer model. Then we quantify the individual contributions of each ISCCP cloud type to the cloud radiative forcing in the region and show that, although individual clouds produce radiative forcings on the order of 100 W m^{-2} , the net effect of the ensemble of clouds is small, as observed. The net radiative neutrality of the deep convective clouds is not a property of a uniform cloud type, but rather is a property of the ensemble of cloud types that is present.

We reason that a feedback process is necessary to enforce the property of radiative neutrality on the cloud ensemble. A heuristic model is developed that includes mechanisms that drive the net radiation in convective areas toward the net radiation in adjoining nonconvective areas. If this feedback operates in nature as it does in our simple model, then it is extremely important that this feedback process be fully understood and faithfully simulated in climate models. Observations of the effect of the cloud ensemble on cloud radiative forcing are described in sections 2–6. A conceptual model of a feedback process to maintain small net cloud radiative forcing is described in section 7.

2. Data

ERBE provides absolutely calibrated “broadband” fluxes of solar and terrestrial radiation at the top of the atmosphere (Barkstrom 1984; Barkstrom et al. 1986; Barkstrom and Smith 1986). The ERBE scene identification algorithm identifies pixels as cloudy or clear, and a separate clear-sky “climatology,” or description of long-term mean conditions, has been developed. The difference between the average of all scenes and the clear-sky climatology is the “cloud forcing,” the radiative effect of clouds on the planetary energy budget. The ERBE data used in this paper consist of daily averages from the scanning instruments (Brooks et al.

1986). The ERBE data from 1985 to 1986 are based on measurements from scanning instruments on two satellites.

ISCCP combines data from geosynchronous and polar-orbiting satellites to produce a global dataset with a $2.5^\circ \times 2.5^\circ$ latitude–longitude grid comparable to the ERBE grid (Schiffer and Rossow 1985; Rossow and Schiffer 1999). The D1 data product contains daily counts of the number of 10-km pixels within each grid that fall into one of 42 cloud types. Cloud types are defined by one of seven cloud-top pressure ranges and six visible optical-depth categories. Each cloudy pixel is assigned to one cloud type, so overlapping clouds are not distinguished.

The analysis in this paper focuses on regions of persistent tropical convective clouds. As a characteristic example we select the region from 0° to 15°N latitude, and 120° to 150°E longitude, during July and August in 1985 and 1986. Similar results could be obtained for other seasons. This area is mostly ocean but includes most of the Philippines, Micronesia, and the Marshall Islands. The large area gives a good sample of data representative of cloud systems and feedbacks on this scale. During boreal summer, the region is heavily covered by deep convective clouds whose net radiative effect is small. Figure 1a shows the ISCCP estimate of fractional area of clouds with cloud-top pressures less than 440 mb and the ERBE estimate of cloud net radiative forcing for the boreal summer season of June–August. The fractional coverage by high clouds is about 55% in the region chosen for study, yet the net cloud radiative forcing magnitude is less than about 10 W m^{-2} (Fig. 1b).

Figure 2 shows the histogram of ISCCP cloud types in the region of interest averaged over the 4-month period of interest. About 15% of the area is covered with clouds in the highest and thinnest ISCCP category corresponding to very thin ice clouds near the tropopause. Clouds with optical depths between 1 and 4 are the most common and cover 25% of the area. The approximate average albedo for clouds in this optical depth category is about 0.3. Also present at upper levels are substantial amounts of cloud with higher optical depths, with about 16% of the area covered by clouds with optical depths greater than 9. These results are conditioned by the pixel size and other limitations of the ISCCP dataset, but we believe they are representative of the general characteristics of clouds in this region, and we believe they are adequate for the demonstration we undertake here.

Figure 3 shows the time series of ERBE observations of reflected shortwave, OLR, net radiation, and ISCCP total cloud cover in the region of interest. The longwave and shortwave show variability of $80\text{--}100 \text{ W m}^{-2}$ in association with cloud cover changes. The ERBE reflected shortwave varies between 68 and 168 W m^{-2} with a mean of 117 and a standard deviation of 23 W m^{-2} . The OLR is anticorrelated with the shortwave (correlation coefficient of -0.95). The OLR has a range

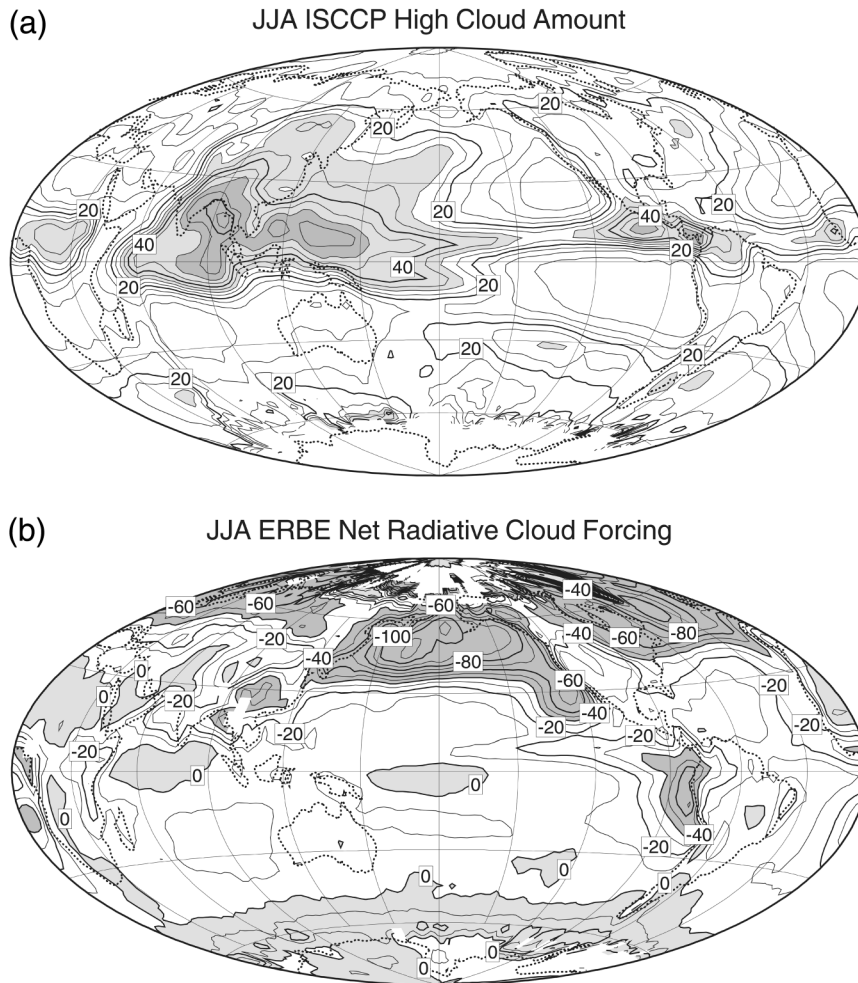


FIG. 1. Equal-area maps for the Jun–Aug (JJA) season. (a) ISCCP 1983–90: climatology of fractional coverage by clouds with tops at pressures less than 440 mb. Contour interval is 5%; values greater than 30% are lightly shaded; values greater than 50% are heavily shaded. (b) ERBE net radiative cloud forcing for 1985–86: contour interval is 10 W m^{-2} ; Positive values are lightly shaded; values less than -30 W m^{-2} are heavily shaded. The latitude and longitude lines are spaced at 30° ; and the date line is in the center of the figure.

between 167 and 253 W m^{-2} , a mean of 211 W m^{-2} , and a standard deviation of 18 W m^{-2} . The degree of cancellation between the effect of clouds on the albedo and the OLR is great. The ERBE net radiation flux is between 79 and 119 W m^{-2} , less than one-half of the OLR or reflected SW ranges. The mean net radiative flux is 96 W m^{-2} with a standard deviation of 8 W m^{-2} .

The net radiation has a smaller short-term variation of 10 – 20 W m^{-2} , with some larger slow variations associated with seasonal and interannual variations. Irradiances show a seasonal trend between 1 July and 31 August. The shortwave reflected irradiance trend in the 1985 period (-16 W m^{-2}) is more than 2 times the trend in the 1986 period (-7 W m^{-2}). The OLR trends for 1985 and 1986 are $+10$ and $+13 \text{ W m}^{-2}$, respectively, for the 2-month periods. Similar to the shortwave trend, the net flux trend in the 1985 period is greater

($+22 \text{ W m}^{-2}$) than that in 1986 ($+10 \text{ W m}^{-2}$). These seasonal trends are removed from the time series when making composite data so that the composites represent variability associated with weather rather than seasonal change.

The time series of total cloud fraction for the study area is given in Fig. 3d. On average it is cloudy 76% of the time. The peaks and troughs correspond with those of the ERBE shortwave flux (correlation coefficient of 0.89) and with the ERBE OLR (correlation coefficient of -0.95). The time average for 1985 is slightly greater than for 1986 (78% vs 73%). The variability in 1985 is less than in 1986—the standard deviations from the mean are 10% and 14%, respectively.

The National Centers for Environmental Prediction–National Center for Atmospheric Research (NCEP–NCAR) reanalysis project provides mapped data from

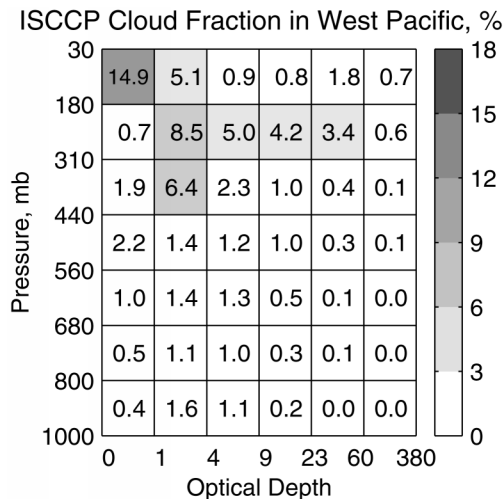


FIG. 2. Average ISCCP cloud-category percent coverage in the region 0° – 15° N, 120° – 150° E during Jul and Aug 1985 and 1986 as a function of cloud-top pressure and optical depth (42 cloud categories).

1948 to the present (Kalnay et al. 1996). Global coverage of numerous parameters is available on a $2.5^{\circ} \times 2.5^{\circ}$ latitude–longitude grid. NCEP–NCAR temperature and humidity profiles averaged over our region and time period of interest are used for the radiative calculations done here. The profiles are given for 17 mandatory pressure levels between 10 and 1000 mb. The maximum temperature (302 K) is at the surface, and the minimum is (193 K) at 100 mb. The freezing point of water occurs at approximately 570 mb. Above 300 mb, no humidity data are provided by the NCEP–NCAR reanalysis. Because the relative humidity from the inversion to 300 mb is approximately 60%, we assume a constant relative humidity of 60% from 300 to 100 mb. Above 100 mb, a constant stratospheric value of 3.8 ppmv was assumed for water.

3. Radiation model

A radiation model developed by Fu and Liou (1992, 1993) is used along with the ISCCP and NCEP–NCAR data to investigate the effects of cloud type and its variation on the radiative energy budgets at the top of the atmosphere. The delta–four–stream approximation is used. The nongray gaseous absorption by H_2O , CO_2 , O_3 , CH_4 , and N_2O is incorporated into the multiple scattering model by using the correlated k -distribution method. The H_2O continuum absorption is included in the spectral region 280 – 1250 cm^{-1} . For water clouds, a parameterization for the single-scattering properties is developed based on Mie calculations using the observed water droplet size distributions in terms of cloud liquid water content and mean effective radius. For ice clouds, a newly developed parameterization of the radiative properties is used that considers nonspherical ice par-

ticles in both the IR and solar spectra (Fu 1996; Fu et al. 1998).

The radiation model generates daily averaged top-of-atmosphere OLR, shortwave reflected, and net flux for each of the ISCCP-defined cloud types. Hourly calculations are done during the day to construct a daily average. The approximately 1.5% seasonal change of top-of-atmosphere insolation over the 2-month period was incorporated by calculating the shortwave irradiances for the mean insolation and then scaling them to the actual insolation on each day.

Our region of interest is predominantly ocean, and we assume 7% albedo and 99% emissivity of the surface. Cloud information needed for the model is matched to the ISCCP categories. Effective cloud particle radii of 30 and $10 \mu\text{m}$ were assumed for ice and water clouds, respectively. Clouds above 560 mb were assumed to be ice. The midpoints of the six ISCCP optical depth bins (0.65, 2.41, 6.46, 16.0, 41.5, and 219.5) and pressure bins (105, 245, 375, 500, 620, 740, and 900 mb) were used for the calculations. The physical cloud depths are climatological values ranging from 1.0 to 4.5 km (Liou 1992). Profiles of the pressure, temperature, and water vapor are taken from the NCEP–NCAR reanalysis dataset described above. The ozone total column, CO_2 , O_2 , and methane concentration values are 275 Dobson Units, 330 ppmv, 28%, and 1.6 ppmv, respectively.

Figure 4 shows the top-of-atmosphere reflected shortwave, OLR, and net radiative flux for each cloud type under overcast conditions. For the second layer from the top, where ISCCP shows the most deep convective cloud tops, the shortwave reflected flux ranges from 70 to 312 W m^{-2} , when going from the lowest to the highest optical depth category. For optical depths greater than about 4, the OLR is almost independent of visible optical depth but depends strongly on cloud-top pressure. The OLR results range from 83 W m^{-2} for the highest, thickest cloud to 277 W m^{-2} for the lowest, thinnest cloud.

The net radiative flux varies between -131 and $+181 \text{ W m}^{-2}$ as a function of height and optical depth (Fig. 4c). The cloud type that results in the most strongly positive net radiation is the highest and second thinnest cloud. The cloud type with the most strongly negative net radiation is the lowest and thickest cloud. The net radiation thus shows a strong gradient from strongly negative to strongly positive when going from low, thick to high, thin clouds.

4. Analysis and validation of cloud radiative forcing

Before discussing the effects of cloud-type distributions on the radiation balance, we must first determine that the combination of ISCCP data with a model gives a good simulation of the ERBE observations. Two metrics are used to evaluate how well our radiation model

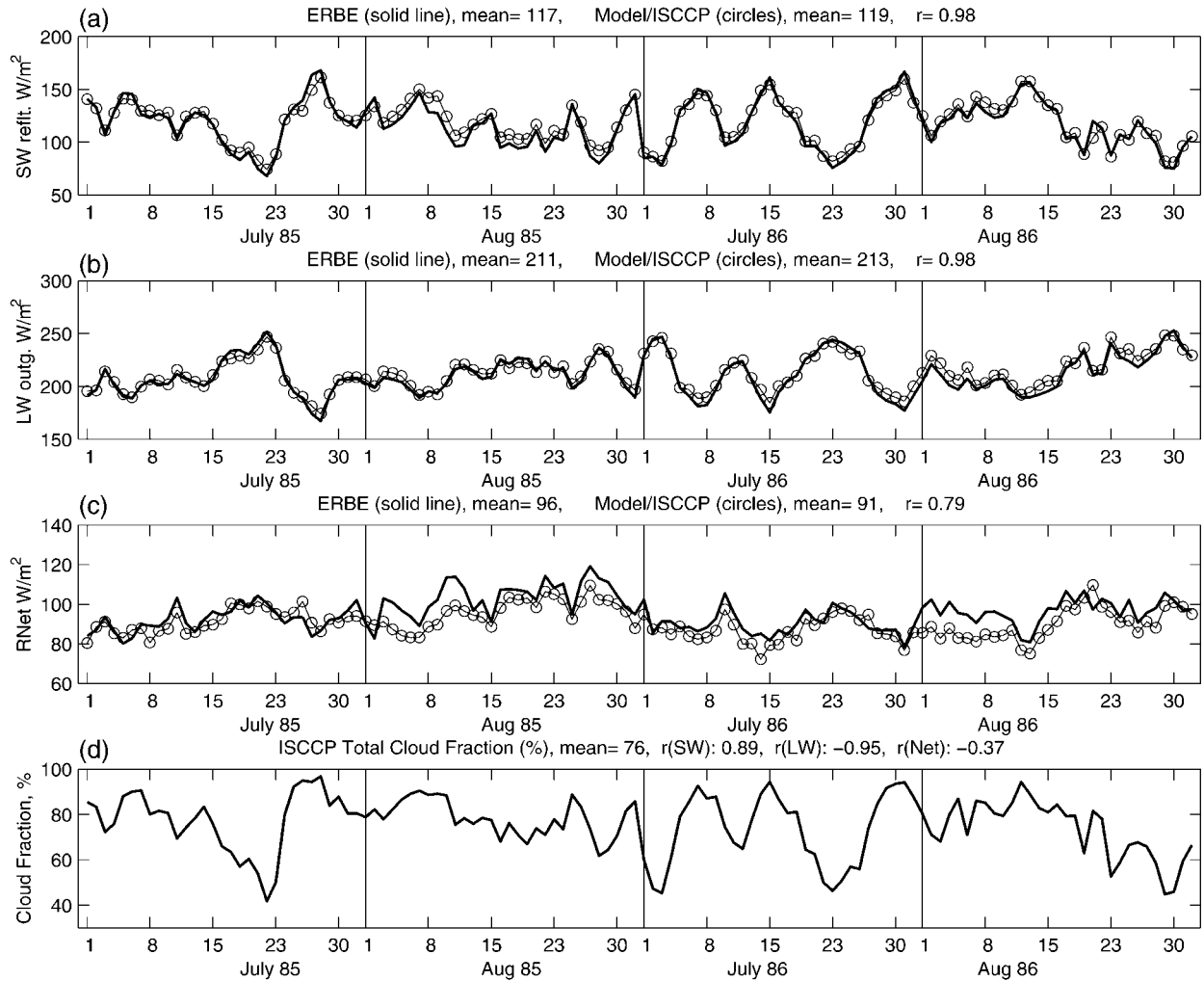


FIG. 3. Time series of ERBE and modeled (a) reflected shortwave, (b) outgoing longwave, and (c) net radiation. (d) Time series of ISCCP total cloud cover averaged for the region 0° – 15° N, 120° – 150° E during Jul and Aug 1985 and 1986.

with ISCCP cloud data simulates the ERBE observations: a comparison of the time series of OLR, reflected solar, and net radiation and a comparison of the estimated total cloud forcing values.

a. Time series comparison

We calculate daily OLR, shortwave, and net radiative fluxes for the region of interest using our radiation model with the ISCCP cloud data. The average irradiance R is obtained by summing the calculated contributions from each cloud type, weighted by their fractional area coverage in the region of interest on each day:

$$R = A_{\text{clear}}R_{\text{clear}} + \sum_{i=1}^{42} A_i R_i, \quad (1)$$

where R_i is the irradiance for the ISCCP cloud type i , A_i is the fractional area coverage of cloud type i , and

R_{clear} is the clear-sky flux. The clear fraction A_{clear} is related to the fractional cloud coverage by

$$A_{\text{clear}} = 1 - \sum_{i=1}^{42} A_i. \quad (2)$$

The fractional area cloud coverage parameters A_i are given by the ISCCP dataset, and the radiative fluxes R_i and R_{clear} are calculated using the radiation model.

Figure 3 shows the daily values of the calculated radiation budget quantities from (1), along with the ERBE observations. In general, the simulated radiative fluxes compare well with the ERBE observations. The correlation coefficients for the reflected SW and OLR between ERBE observations and the simulated time series are both 0.98. The time-averaged ERBE observations minus the simulated time series are $+2.3 \text{ W m}^{-2}$ (2%) and $+2.3 \text{ W m}^{-2}$ (1%) for the reflected SW irradiance and OLR, respectively.

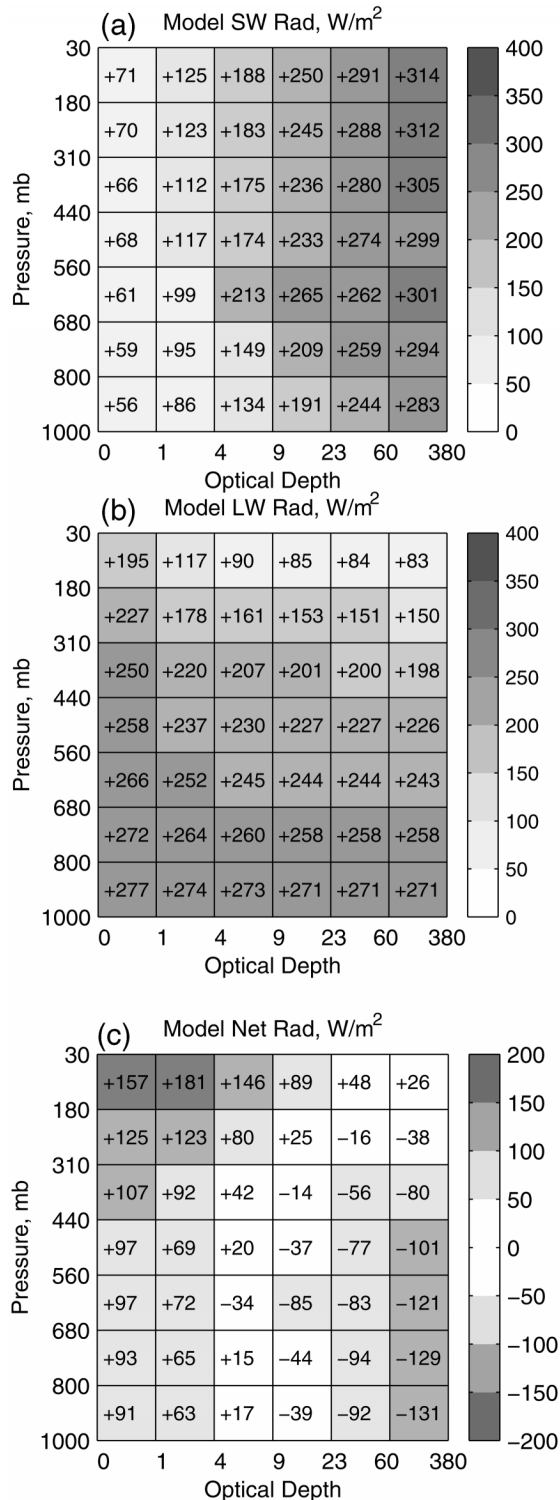


FIG. 4. Calculated (a) shortwave, (b) longwave, and (c) net radiation for each of the 42 ISCCP cloud categories for the region 0° – 15° N, 120° – 150° E during Jul and Aug 1985 and 1986.

The OLR is affected by the water vapor distribution in the atmosphere, including the heights at which there are no NCEP humidity data. As a sensitivity study, we varied the water vapor values between 40% and 80% in the levels at which NCEP does not provide data (100–300 mb). In the OLR clear-sky values there is a $5 W m^{-2}$ decrease, and in the OLR full-sky values there is a $3 W m^{-2}$ decrease. These changes are comparable in magnitude to the uncertainty in the ERBE data. A more detailed analysis could include observed daily variations of temperature and humidity at high spatial resolution, but for the current purposes it is adequate to use constant temperature and humidity averaged over the region of interest.

The agreement of the calculated net radiation with the ERBE observations is not as good as the comparisons with shortwave and longwave irradiances. This result is simply because the net radiation variations are small differences between two larger and opposing variations in shortwave and longwave. The correlation coefficient between the time series of ERBE and modeled net radiation is about 0.79. The mean model net radiation is $4.6 W m^{-2}$ less than the mean ERBE observations, about a 5% difference. This mean difference is nonetheless within the uncertainty of the ERBE measurements.

b. Net radiation and cloud forcing

The net radiation is the difference between absorbed solar radiation and outgoing longwave radiation measured at the top of the atmosphere:

$$R = S^{\downarrow} - S^{\uparrow} - F^{\uparrow} = S^{\downarrow}(1 - \alpha) - F^{\uparrow}. \quad (3)$$

Here, S^{\downarrow} is the insolation and α is the albedo. The net cloud radiative forcing is defined to be the change in the net radiation associated with the clouds, all else being equal:

$$\Delta R = R - R_{\text{clear}}. \quad (4)$$

Because the reflected solar radiation S^{\uparrow} and the OLR F^{\uparrow} occur with negative signs in the equation for net radiation [(3)], decreases in reflected solar or OLR are increases in net radiation R . This relation needs to be kept in mind in interpreting results shown below.

c. Overcast-sky cloud forcing

The difference between the top-of-atmosphere irradiances of a sky completely covered by one cloud type and a completely clear sky is the “overcast-sky cloud forcing” for each cloud type. The overcast-sky cloud forcing for a particular cloud type i (ΔR_i^{oc}) is given by

$$\Delta R_i^{\text{oc}} = R_i - R_{\text{clear}}. \quad (5)$$

Figure 5a shows the net cloud forcing for a sky overcast by each of the ISCCP cloud types for the mean conditions of the region of interest. The calculated clear-

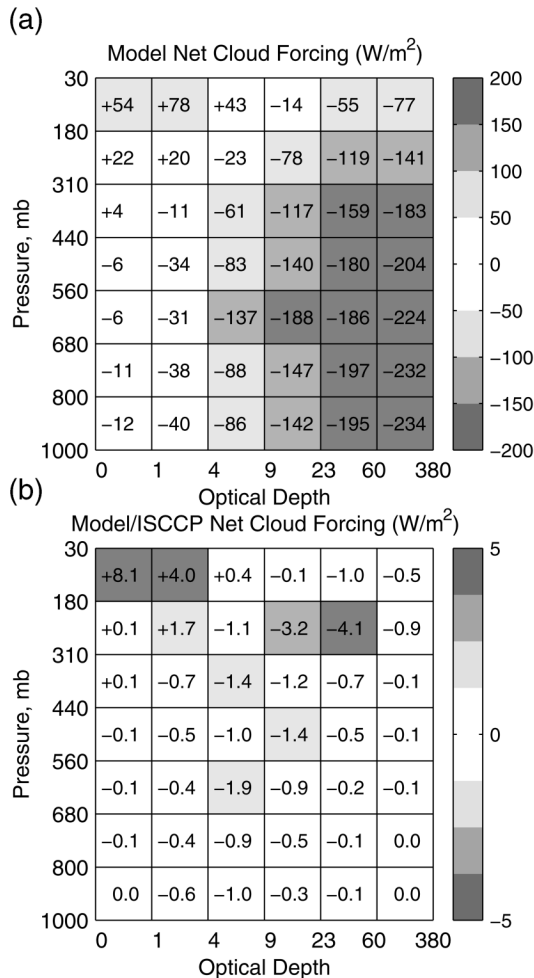


FIG. 5. (a) Modeled overcast-sky net cloud radiative forcing and (b) modeled average-sky net cloud forcing for each of the ISCCP cloud categories for the region 0° – 15° N, 120° – 150° E during Jul and Aug 1985 and 1986 ($W m^{-2}$).

sky net radiation value ($103 W m^{-2}$) is greater than that of most of the cloud types. So, the cloud forcing for most cloud types has a cooling effect (-6 to $-234 W m^{-2}$). Only 6 of the 42 cloud types have a warming effect, and they are the higher, thinner clouds. The highest and thinnest cloud type, which is the most common type, has a large positive overcast-sky net forcing of $54 W m^{-2}$.

d. Average-sky cloud forcing

“Average-sky” is a term to indicate the observed mixture of clear and cloudy scenes, in this case characterized by the average ISCCP cloud distribution (Fig. 2). The “average-sky cloud forcing” is a useful measurement that describes the response of the radiation field to the observed distribution of clouds and should be comparable to the cloud forcing estimated by ERBE. As actually measured, ERBE cloud forcings may in-

clude differences in temperature and humidity associated with cloud coverage. In the calculations done here, however, cloudy and clear scenes are given the same temperature and humidity profiles. The contribution to the average-sky cloud forcing by an individual cloud type (ΔR_i^{ave}) is given by the product of the overcast-sky cloud forcing by that cloud type and the fractional area coverage by that cloud type A_i :

$$\Delta R_i^{ave} = A_i(R_i - R_{clear}). \quad (6)$$

The simulated individual average-sky cloud forcing is presented Fig. 5b. Note the opposing effects of the highest thinnest cloud and the bright anvil cloud with optical depths between 4 and 60. The total positive cloud forcing is $14 W m^{-2}$, dominated by the two highest and thinnest types ($+8.1$ and $+4.0 W m^{-2}$, respectively) which have the effect of warming the planet. The total negative cloud forcing is $-25 W m^{-2}$, with the largest contributions of -3.2 and $-4.1 W m^{-2}$ coming from high, thick anvil cloud. Substantial negative cloud forcings in the -1 – $-2 W m^{-2}$ range come from optically thick clouds (optical depths between 4 and 23) with tops below 310 mb. The five categories with positive cloud radiative forcings cover about 32% of the area of the region of interest, and clouds with negative cloud forcing cover about 42% of the region.

e. Comparison of average-sky cloud forcing

The reflected shortwave, longwave, and net radiation for average-sky and clear-sky and their implied cloud forcing values are listed in Table 1, both for the ERBE observations and the calculated values. The differences between the ERBE radiative flux observations and the simulations are all within $4 W m^{-2}$. The net cloud forcing, the difference between the average-sky and clear-sky values, is small and negative, with the calculated value slightly larger (ERBE: $-7 W m^{-2}$; model: $-11 W m^{-2}$). The differences between the observations and the simulations could be attributed to inaccuracies in the ERBE, ISCCP, and NCEP data, or inaccuracies in the model simulations. The magnitudes of the differences are within the measurement uncertainty of the ERBE data, and it is not worth pursuing them further here. The data and model agree well enough to warrant further comparison.

5. Composite analyses

Within the region and time frame of interest here, the cloud coverage and radiation budget quantities vary significantly. In this section, we investigate this variability by compositing the ISCCP cloud categories relative to the ERBE radiation budget quantities. We search the detrended ERBE dataset for days on which the irradiance is one standard deviation σ above or below its mean value. We then obtain six sets of dates for low and high values for ERBE shortwave, longwave, and

TABLE 1. ERBE and modeled radiation balance components for the west Pacific convective region 0° – 15° N, 120° – 150° E ($W m^{-2}$).

	Longwave		Shortwave		Net radiation	
	ERBE	Model	ERBE	Model	ERBE	Model
Average sky	211	213	117	119	96	92
Clear sky	280	278	40	42	103	103
Cloud forcing	70	65	-77	-77	-7	-11

net radiation. With these six sets of dates, we construct composite averages of ISCCP cloud coverage. The “low” composite averages are subtracted from the “high” composite averages to get “high-minus-low” changes in ISCCP cloud distribution associated with significant changes in each of shortwave, longwave, and net radiation. The composites are averages of approximately 20 days selected from the 124-day study period. The average ERBE fluxes for these key dates are also computed.

The ISCCP cloud distribution changes associated with $\pm 1 \sigma$ changes in ERBE shortwave, longwave, and net radiation are shown in Figs. 6a–c, respectively. In each case, one observes an anticorrelation between upper-level and lower-level clouds. The screening of lower-level clouds by upper-level clouds influences this anticorrelation when observations are taken from space, and we will focus mostly on the changes in upper-level clouds. The differences in Fig. 6 can be compared with the mean cloud cover given in Fig. 2. The largest composite differences in cloud coverage associated with ERBE shortwave and longwave variations occur for the clouds with the largest climatological abundance. This reflects the fact that most of the upper-level cloud types are associated with mesoscale convective cloud complexes, and so all the cloud types vary in synchrony. One significant exception to this rule is the highest, thinnest cloud type, which varies proportionately much less than the other cloud types. The high, thin cirrus may be related more to the coldness of the tropopause than to the presence of nearby deep convection. Moreover, the detection of thin cirrus overlapping thicker anvil cloud below is difficult with the two channels that ISCCP uses. So, an increase of cirrus during periods of active convection may be masked by the smaller fraction of the area in which cirrus could be detected by ISCCP if they were present. The ISCCP cloud distribution responses to shortwave and longwave compositing are almost mirror images of each other, which is consistent with the high degree of cancellation between longwave and shortwave effects of deep convective cloud complexes. In the case of the shortwave and longwave composites, the total cloud cover varies substantially by 34% and 36%, respectively.

When the ISCCP data are composited with respect to ERBE net radiation, the total cloud cover change is smaller, 19% as compared with about 35%. When the data are composited for high values of ERBE net radiation, high, optically thick clouds decrease more, as

a percentage of their climatological abundance, than do clouds at the same altitude with smaller visible optical depths. So, while net radiation increases when the amount of convective cloud decreases, it also responds sensitively to shifts in the relative frequency of optically thick and thin high clouds. The importance of the shift from thin to thick anvil clouds for the radiation balance can be confirmed by applying (4) using the cloud-type differences in Fig. 6 (not shown).

6. East Pacific convection

Figure 1 shows that in the eastern Pacific ITCZ region centered near 10° N and 120° W, the convective clouds produce a significantly negative net cloud forcing with magnitude in excess of $20 W m^{-2}$. We have performed a similar analysis to that above for an east Pacific ITCZ region (7.5° – 15° N, 100° – 140° W). The ISCCP cloud histogram for July–August 1985 and 1986 is shown in Fig. 7. By comparing this figure with the histogram for the west Pacific region in Fig. 2 it can be seen that the east Pacific has less optically thin cloud relative to optically thick upper cloud as well as more mid- and low-level cloud. These differences are maintained if one calculates a conditional probability in which one asks what fraction of the area that is not obscured by upper clouds is occupied by clouds at each level.

The radiation comparison for the east Pacific region is given in Table 2. The agreement between the ERBE data and the model calculation using ISCCP and NCEP data is not as good as in the west Pacific. In particular, the calculation indicates a cloud radiative forcing of $-44 W m^{-2}$ as compared with the ERBE estimate of $-24 W m^{-2}$. Nonetheless, both ERBE and the calculation indicate a strongly negative cloud forcing. This change to more negative cloud forcing is associated with both a reduction in longwave cloud forcing (ERBE: -13 , model: $-16 W m^{-2}$) and an increased negative shortwave cloud forcing (ERBE: -5 , model: $-16 W m^{-2}$). So, the clouds in the east Pacific convective region are both warmer and brighter than those in the west Pacific region. Convective clouds in the east Pacific are known to be very different in structure from those in the west Pacific. They tend to have less high anvil and cirrus cloud and produce more rain per unit of OLR anomaly than do west Pacific convective clouds (Yuter and Houze 2000). East Pacific convection may be affected by the proximity of cool SST on the equator and is more strongly forced by concentrated upward motion

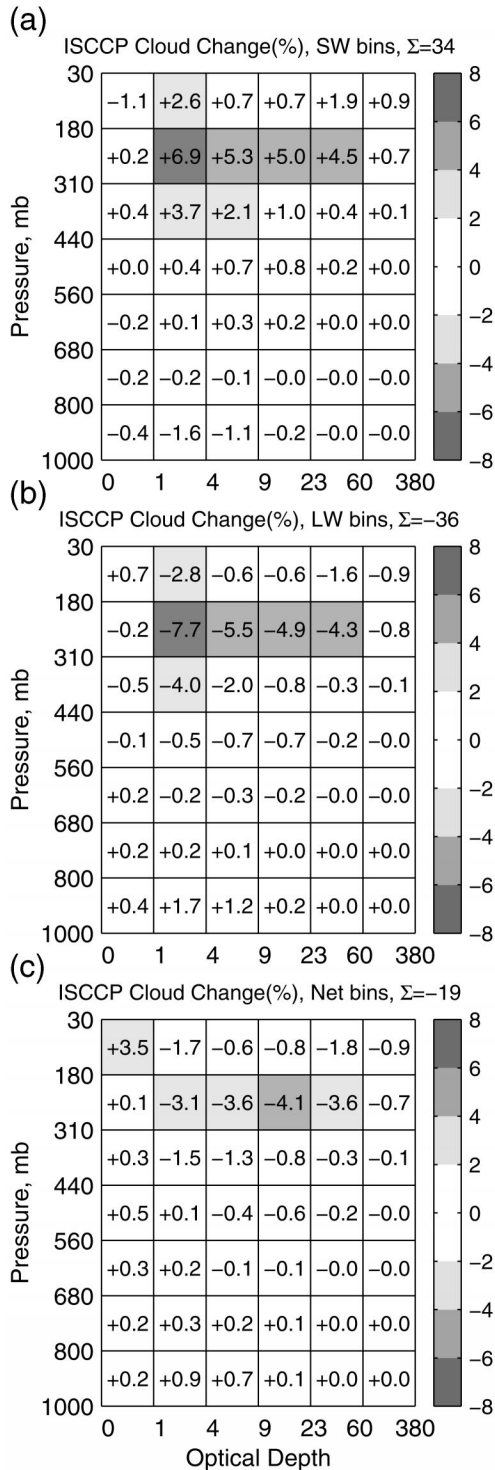


FIG. 6. Changes in ISCCP cloud fractions associated with ± 1 -sigma changes in ERBE (a) shortwave, (b) longwave, and (c) net radiation in the region 0° – 15° N, 120° – 150° E during Jul and Aug 1985 and 1986.

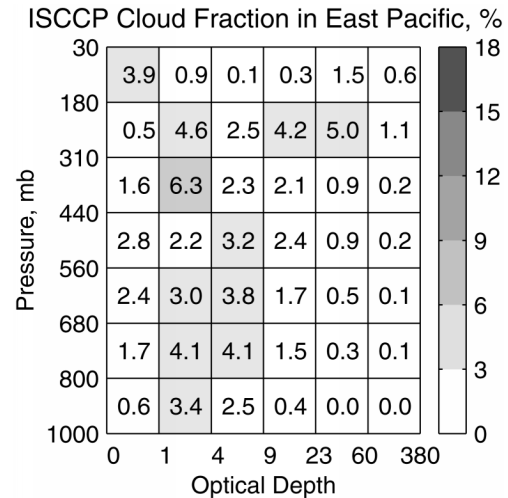


FIG. 7. Same as Fig. 2 but for the region 7.5° – 15° N, 100° – 140° W.

along the narrow band of high SST in the eastern Pacific. The intense convection over the miniature warm pool west of Mexico, which is a greater expanse of warm water farther away from the equatorial upwelling, does show the small net radiative effect observed for west Pacific convective clouds. The model described in the following section suggests a possible explanation for the negative radiative forcing of clouds in the east Pacific ITCZ.

7. A simple feedback model

a. The concept

We begin with a thought experiment and ask what would happen if convective clouds did develop a sustained anomaly in the net radiation as compared with nearby regions. If, for example, the net radiative effect were negative, then the region would begin to lose energy relative to adjacent regions. The result of this would have to be a reduction in the intensity of the deep convection in the region of interest and a corresponding reduction in the average optical depth of the clouds. Either the temperature would have to decrease in the convective region, or an anomaly in the circulation would have to develop to compensate the loss of energy. To transport energy into the convective region would require subsidence in the convective region, which would quickly suppress convection. The response to a reduction in net radiation would be a reduction in cloud albedo, which would drive the net radiation back toward more positive values. If the clouds produced a positive net radiation anomaly, then this would lead to intensified convection, raising the average optical depth of the clouds and leading again to a negative feedback. This basic feedback mechanism can operate on a wide range of spatial and temporal scales.

One may ask why we have focused on the optical

TABLE 2. ERBE and modeled radiation balance components for the east Pacific convective region 7.5°–15°N, 100°–140°W ($W m^{-2}$).

	Longwave		Shortwave		Net radiation	
	ERBE	Model	ERBE	Model	ERBE	Model
Average sky	227	229	124	136	78	66
Clear sky	284	279	43	42	103	110
Cloud forcing	57	49	-82	-93	-24	-44

depth of the clouds and the associated shortwave cloud forcing rather than on the longwave effect of the clouds, given that Figs. 2 and 4c suggest a strong dependence of net radiation on cloud-top altitude. First, the shortwave feedback is clearly negative and so will lead to a stable equilibrium. Longwave feedback can lead to either negative or positive feedback, depending on whether the atmospheric heating produced by these clouds is expressed as a temperature increase (stabilizing) or a vertical motion increase (destabilizing). In limited area models, the longwave effect can be stabilizing (Fu et al. 1995). If the longwave heating can be easily exported by circulations, however, then the upward motion in the heating area can enhance the cloud coverage or altitude. If the longwave feedback were negative, as in Fu et al. (1995), then it would work like the shortwave feedback we consider here, because the longwave effects of the clouds would reduce convection and the associated circulation.

Another reason for focusing on the albedo effect of clouds is that the albedo is more variable than the cloud-top temperature. The maximum abundance of optically thick cloud is actually below the tropopause, closer to the 200-mb level (Fig. 2). These clouds are stratiform anvil clouds and may be the key cloud types in determining the net radiative effect of convective cloud complexes. The anvil cloud covers a large area and has a wide range of optical thickness. The development of extended anvil cloud is favored in areas of intense convection where convective updrafts are closely spaced (Houze 1993, see chapter 9). The concentration of anvil clouds near 200 mb may be a result of the abrupt decrease of clear-sky radiative cooling at this altitude. At temperatures colder than those of the tropical atmosphere near 200 mb, the water vapor pressure is sufficiently small that cooling by emission from rotational bands of water vapor becomes inefficient, and clear-sky radiative cooling cannot balance strong convective heating (Hartmann et al. 2001). Therefore convective cloud decreases abruptly above this level, and anvil clouds tend to concentrate at this level.

The direct radiative effect of solar absorption by the cloud on the cloud structure is likely to be fairly modest. Solar absorption in clouds may evaporate some cloud particles and provide some heating near the top of the clouds, but these effects seem inadequate to maintain discipline over rapidly evolving cloud populations. The most powerful influence of the clouds on shortwave radiation is to reduce the insolation reaching the surface, because most of the shortwave cloud forcing is felt there. Ramanathan and Collins (1991) have used these arguments to suggest that the albedo effect of tropical convective anvil clouds places an upper limit on tropical SST of 305 K. Here we use the same facts to argue that a feedback effect of tropical cloud optical thickness is to drive the net radiation in convective and nonconvective regions toward the same value. If the cloud radiative forcing in the nonconvective regions is small, then this requires that the cloud radiative forcing of the convective cloud ensemble also be small.

To use the equality of net radiation in convective and nonconvective regions to imply that cloud forcing in convective regions should be small, we must first demonstrate that the cloud radiative forcing in nonconvective areas is equally small. We have tested this in two ways. We have taken the climatological ISCCP data from a large region where convection is scarce in the equatorial Pacific, sometimes called the Great Oceanic Desert or "dry zone" because precipitation is so rare there. If we take the region from 0° to 15°S and from 130° to 150°W we get an average cloud fraction of 35%, most of which is low cloud. Using our model we get a net cloud forcing of $-10 W m^{-2}$ (Table 3), which is small and very close to the value of $-11 W m^{-2}$ calculated for the convective region in the west Pacific (Table 1). In doing the calculation for the dry zone, we reduced the relative humidity above the inversion to 20% to get the calculated clear-sky longwave irradiance to agree with the ERBE value, but this adjustment does not affect the cloud forcing. The NCEP-NCAR humidities may be unrealistically high in this region. The cal-

TABLE 3. ERBE and modeled radiation balance components for the central Pacific dry-zone region 0°–15°S, 130°–150°W ($W m^{-2}$).

	Longwave		Shortwave		Net radiation	
	ERBE	Model	ERBE	Model	ERBE	Model
Average sky	296	293	54	58	34	31
Clear sky	301	301	43	40	38	41
Cloud forcing	5	8	-10	-19	-4	-10

culated cloud reflectivity is larger than the ERBE data suggest for both the central and east Pacific regions.

We also took the ISCCP data for the west Pacific region and searched for days with low total cloudiness. For each 2.5° grid box in the 0° – 15° N, 120° – 150° E region, we searched for daily cloud fractions less than 50% and averaged these days together. About 20% of the data passed this criterion and had an average cloud cover of 32.4%. The net cloud forcing for this sample was calculated to be -1.4 W m^{-2} , very close to zero. This was composed of a negative forcing from low clouds of -8.8 W m^{-2} and a positive forcing of 7.4 W m^{-2} from high, thin clouds. So, we conclude that, whether one uses climatological values for nonconvective regions or one takes nonconvective days from within a convective region, very small net cloud radiative forcing is obtained for nonconvective conditions. In convective regions, the small radiative cooling by trade cumulus clouds is offset by the effect of persistent thin clouds near the tropopause. Even without the effect of tropopause cirrus, however, the low cloud forcing in convective regions on nonconvective days is less than about 10 W m^{-2} .

A potential problem with using the effect of clouds on surface solar heating to constrain the optical properties of clouds is the very short timescale on which convective cloud structures evolve as compared with the longer response time of the upper ocean and SST. Tropical convective systems can develop and regenerate on timescales of less than a day. Average mixed-layer depths in the tropical oceans are sufficient to give relaxation timescales of weeks for SST. Moreover, convective systems tend to be of small scale and mobile and can move away from their local effects on surface temperature. If climatological averages show small net radiative forcing for tropical convective clouds, then it must also be true for individual convective systems, given that these systems evolve on timescales of less than a day and on spatial scales that are often less than 100 km. Kiehl and Ramanathan (1990) showed that tropical convective clouds have small net radiative forcing even on short time- and space scales.

Although they evolve quickly, the structure of mesoscale cloud complexes in the Tropics is heavily influenced by the mean thermodynamic and dynamic environment of the atmosphere in which they evolve. Key indicators of this environment are the SST, temperature and humidity profiles, and the large-scale vertical motion. So, although tropical cloud complexes evolve quickly, their statistical properties are governed by large-scale factors that evolve on longer timescales. If a feedback is to exist between the top-of-atmosphere net radiative effect of clouds and cloud structure, then the memory must reside in the SST and the atmospheric temperature and humidity profiles. The timescale at which these interactions can proceed may be much shorter than the timescales required to change oceanic mixed-layer structure, if the system is already close to

equilibrium. Chen and Houze (1997) have documented the importance of radiative effects of clouds in suppressing convection even on short time- and space scales. They suggested that the occurrence of deep convection on one day can leave a cooled boundary layer and SST that disfavor convection on the following day.

b. A "toy" model

We propose here a simple heuristic model that shows how the net radiation at the top of tropical convective cloud complexes is constrained by a feedback process. The model is based on three basic observations.

- 1) SST gradients in the Tropics are small. Within the warm-pool region of the western Pacific and Indian Ocean where convective cloud complexes are common, the SST varies only by a few degrees Celsius. This means that gradients in moist static energy are weak.
- 2) ISCCP data suggest that the tops of optically thick convective clouds occur most frequently in the ISCCP category between 310 and 180 mb. For clouds with tops in this range, the optical depth can vary between 1 and 60, yielding a wide range of cloud albedos.
- 3) The albedo of tropical convective clouds is very sensitive to the large-scale convergence and vertical velocity, and to small gradients in SST. Ramanathan and Collins (1991) used observations to estimate a sensitivity of absorbed solar radiation to SST variations of $-25 \text{ W m}^{-2} \text{ K}^{-1}$. Hartmann and Michelsen (1993) argued that this was mostly a response of clouds and circulation to changing horizontal distributions of SST, rather than to the absolute value of SST, the maximum value of which does not change much. They found that the sensitivity of the tropical-average albedo to the tropical-average SST is very weak. Lau et al. (1994) used a cloud-resolving model to show that the cloud albedo was much more sensitive to mean vertical motion than to the absolute value of the SST (see also Tompkins and Craig 1999).

From these observations we may conclude that the albedo of tropical convective clouds is sensitive to SST gradients and will act to reduce them. What is perhaps less obvious is that the net radiation at the top of the convective clouds is also driven toward the net radiation balance of the adjoining nonconvective areas by these interactions. The degree to which the net radiation in the convective areas must match that in the nonconvective areas depends on the sensitivity of the mean vertical motion to SST gradients, the sensitivity of cloud albedo to vertical motion, and the efficiency with which large-scale motion can move energy horizontally in the deep Tropics. In regions with relatively uniform SST, the efficiency of atmospheric motions in transporting energy by circulation cells is reduced, and the net ra-

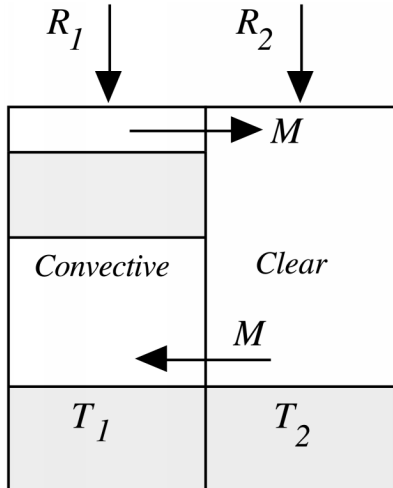


FIG. 8. Schematic diagram of the two-box model.

diation balance in convective and nonconvective areas must be similar.

To illustrate these concepts, we use a very simple two-box model of the atmosphere–ocean system, as illustrated in Fig. 8. The column energy budgets for the convective and nonconvective regions are given by

$$c \frac{dT_1}{dt} = R_1 - \frac{M}{A_1} c_p \Delta \theta_e - \text{Exp}_1 \quad \text{and} \quad (7)$$

$$c \frac{dT_2}{dt} = R_2 + \frac{M}{A_2} c_p \Delta \theta_e - \text{Exp}_2. \quad (8)$$

Here T_1 and T_2 are the SSTs in the convective and nonconvective regions, respectively. These equations should have an atmospheric heat storage term on the left, but this term is negligible because the heat capacity of the atmosphere is small when compared with that of the ocean mixed layer, c . Moreover, in this paper we will consider only equilibrium solutions for which the storage term is zero, but these solutions are obtained by time integration of (7) and (8). Variables R_1 and R_2 are the net radiation at the top of the atmosphere in the two regions, M is the mass flux between the two regions (kg s^{-1}), and $\Delta \theta_e = \theta_{e1} - \theta_{e2}$ is the difference in equivalent potential temperature for saturated air in contact with the surface in each region. As in Larson et al. (1999), we assume that the moist static energy in the free troposphere is approximately that of the air in the boundary layer of the convective region. The energy transport between the boxes is then the mass flux of the overturning cell times the difference of moist static energy of the air near the surface in the two regions. The two regions are assumed to have areas of A_1 and A_2 , respectively. By mass continuity then, the characteristic pressure velocities in the two regions are related by $\omega_1 = -(A_2/A_1)\omega_2$, and the mass flux by the overturning cell between the two regions is $M = A_2(\omega_2/g) = -A_1(\omega_1/g)$. The term Exp is a constant net energy export

to other regions not included in the model domain. It is set to 80 W m^{-2} , which is equal to the average net radiation at the top of the atmosphere in the warm Tropics (e.g., Hartmann 1994). This term is necessary to get realistic net radiation and SST for the Tropics.

In equilibrium, the system defined by (5)–(6) requires that,

$$R_1 - R_2 = M c_p \Delta \theta_e \left(\frac{1}{A_1} + \frac{1}{A_2} \right) + (\text{Exp}_1 - \text{Exp}_2). \quad (9)$$

Thus, in equilibrium the difference in the radiation balance between the two regions depends on the magnitude of the energy transport from the convective to the nonconvective region and on any differences in the export term. In the deep Tropics in regions of expansive warm SST, we will assume that the export terms are the same for the two regions, so that the last term in (9) drops out. We are assuming that, to first order, the radiative properties of tropical convective clouds can be understood in terms of interactions with nearby regions in the Tropics, while using a constant energy export to characterize the remote interaction with the extratropics.

The radiation balance in each region is given by

$$R_i = S(1 - \alpha_i) - F_i, \quad (10)$$

where F is the OLR. In the nonconvective region we use $F_2 = F_{02} + b(T_2 - 300)$, with $F_{02} = 280 \text{ W m}^{-2}$, $b = 2.0 \text{ W m}^{-2} \text{ K}^{-1}$, and an albedo of $\alpha_2 = 0.1$. These correspond to observed clear-sky values (Ramanathan et al. 1989; Harrison et al. 1990), and give the observed net radiative input of 80 W m^{-2} , if the daily average insolation is taken to be $S = 400 \text{ W m}^{-2}$. In the convective region, a lower base value of OLR is given and the same weak linear dependence on temperature is assumed, $F_{01} + b(T_1 - 300)$. The seasonal mean OLR in the convective portions of the west Pacific and Indian Ocean regions is about 190 W m^{-2} (Hartmann 1994). The value of b does not have a significant effect on our interpretation of the model.

The albedo in the convective region will be specified to be a function of the vertical velocity and SST:

$$\alpha_1 = \alpha_2 - \lambda \omega_1 q^*(T_1), \quad (11)$$

where $q^*(T_1)$ is the saturation water vapor mixing ratio at the temperature of the ocean in the convective region. The vertical velocity and corresponding mass circulation are assumed to be proportional to the temperature contrast between the convective and nonconvective regions:

$$\omega_1 = -\gamma(T_1 - T_2) = -\gamma \Delta T. \quad (12)$$

c. Model parameters

The behavior of this model depends on the two constants λ and γ in (11) and (12), which measure the sensitivity of cloud albedo to vertical motion and the sensitivity of the vertical velocity to the temperature

contrast between the regions. If each of these sensitivities is large enough, then the radiation balance of the convective region is driven near the radiation balance of the nonconvective region. One could attempt to model the dependence of the mass circulation on SST gradients as in Lindzen and Nigam (1987) and Hartmann and Michelsen (1993). The Lindzen and Nigam (1987) model includes two parameters and does not explicitly take into account the role of convection in driving circulations in response to SST gradients. Here we will try to get by with one free parameter γ , which we will estimate from observations. The mean vertical velocity in the convective regions of the west Pacific is on the order of $3 \times 10^{-2} \text{ Pa s}^{-1}$ (Schubert et al. 1990). If we assume that this vertical motion is a response to SST differences on the order of 6 K, then γ is about $5 \times 10^{-3} \text{ Pa s}^{-1} \text{ K}^{-1}$. A scatter diagram of 200-mb divergence versus SST shown in Hartmann and Michelsen (1993) suggests a similar order of magnitude. A 200-mb divergence contrast of $6 \times 10^{-6} \text{ s}^{-1}$, if spread over a 500-mb layer, gives a vertical velocity range of about $3 \times 10^{-2} \text{ Pa s}^{-1}$, for observations from an area in which the SST range is about 6 K (their Fig. 2).

To estimate the dependence of albedo on vertical velocity, we can take the mean albedo contrast between convective and nonconvective regions of about 0.25 and divide it by the vertical velocity contrast to yield $\Delta\alpha/\Delta\omega \approx 1.25 \times 10^2 (\text{Pa s}^{-1})^{-1}$. From (11) we can show that

$$\lambda = \frac{1}{q^*} \frac{\Delta\alpha}{\Delta\omega}, \quad (13)$$

so that $\lambda = 5 \times 10^3 (\text{Pa s}^{-1} \text{ kg}_{\text{H}_2\text{O}} \text{ kg}^{-1})^{-1}$, if $q^* = 2 \times 10^{-2} \text{ kg}_{\text{H}_2\text{O}} \text{ kg}^{-1}$.

We are now ready to explore the solutions to the system defined by (7)–(12). We will begin by setting the convective area fraction to 0.3 and the OLR in the convective region to 190 W m^{-2} and will explore the sensitivity of the equilibrium solutions for SST and net radiation to the specification of the parameters γ and λ . On the basis of climatological values of SST, vertical velocity, and albedo in the western Pacific region we have order-of-magnitude estimates of $\gamma = 5 \times 10^{-3}$ and $\lambda = 5 \times 10^3$. We can investigate the sensitivity of the model to variations of the parameters in this range. Figure 9a shows model solutions for $\gamma = 4 \times 10^{-3}$, which is 80% of our order-of-magnitude estimate, as a function of λ varying from 250 to 8000. For values of λ greater than about 500, the net radiations obtained in the two boxes are within 10 W m^{-2} of each other. For lower values of γ , the surface temperatures climb and the net radiations diverge, because the response of the circulation to the temperature differences is weak and the cloud albedo in the convective region does not rise to compensate the low OLR there. Figure 9b shows model solutions for $\lambda = 4000$, which is 80% of the order-of-magnitude estimate given above, as a function of γ ,

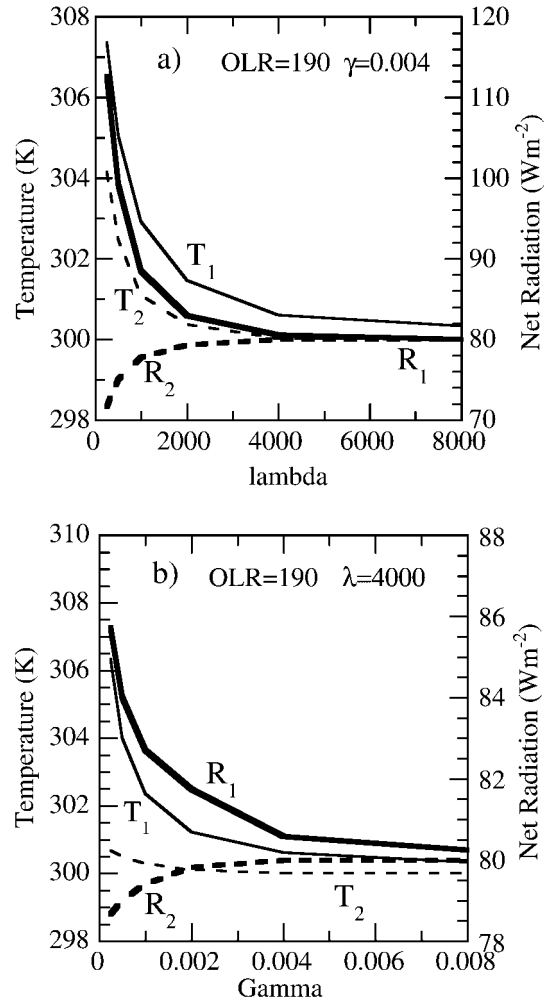


FIG. 9. Model solutions for SST and net radiation for convective (subscript 1) and nonconvective (subscript 2) regions of the two-box model: (a) $\gamma = 0.004$ as a function of λ and (b) $\lambda = 4000$ as a function of γ .

ranging from 2.5×10^{-4} to 8×10^{-3} . For very small values of γ , the temperature also rises and the net radiations diverge—this time because the sensitivity of albedo to circulation is large enough but the circulation does not respond very strongly to the SST difference.

The values of γ and λ obtained above from climatological gradients are just order-of-magnitude assessments. An estimate of the sensitivity of albedo to SST gradient can be taken from the work of Ramanathan and Collins (1991). They estimated the sensitivity of absorbed solar radiation to SST variations by comparing the absorbed solar radiation and SST changes associated with interannual SST variations in the Pacific and obtained a sensitivity of absorbed solar radiation to SST variations of $-25 \text{ W m}^{-2} \text{ K}^{-1}$. If we divide this sensitivity by the mean tropical insolation of 400 W m^{-2} , we obtain $\Delta\alpha/\Delta T = 0.04 \text{ K}^{-1}$. We can combine our

estimates of γ and λ to obtain an estimate of the sensitivity of the albedo to temperature. From (11) and (12),

$$\Delta\alpha/\Delta T = \lambda\gamma q^*. \quad (14)$$

If we use a value of $q^* = 0.02 \text{ kg}_{\text{H}_2\text{O}} \text{ kg}_{\text{air}}^{-1}$, then the $-25 \text{ W m}^{-2} \text{ K}^{-1}$ estimate of the sensitivity of reflected shortwave to SST variations implies that the product of γ and λ should be about 2. We will see that if we constrain the parameters in our model such that $\gamma\lambda = 2$, so that $\Delta\alpha/\Delta T = 0.04 \text{ K}^{-1}$, we obtain a feedback that is easily strong enough to bring the net radiation in the convective region near to that in the adjoining nonconvective regions. The use of this estimate implies that we are considering scales of circulation comparable to those associated with the changes in circulation associated with ENSO events. Hartmann and Michelsen (1993) showed patterns with changes of albedo of opposite sign separated by about 15° of latitude in the central Pacific. We can say that 1500 km is the approximate scale implied for the separation between the convective and nonconvective boxes in this problem and for the corresponding SST, albedo, and net radiation changes that the model will produce. Both boxes are in the deep Tropics, and the SST difference between them is a few degrees. The model should produce SST and albedo contrasts that are comparable to the observed ones used to scale γ and λ .

We next show results obtained by assuming the albedo sensitivity to SST found empirically by Ramanathan and Collins (1991), which implies that we should keep the product $\gamma\lambda = 2 \text{ (K kg}_{\text{H}_2\text{O}} \text{ kg}^{-1})^{-1}$, so that $\Delta\alpha/\Delta T = 0.04 \text{ K}^{-1}$. Figure 10a shows the results of varying λ while also varying γ to keep $\gamma\lambda = 2$ for the case with the convective region OLR set to 190 W m^{-2} . For small values of λ , in which case the cloud albedo is insensitive to vertical velocity, the net radiations in the two regions diverge, and the temperatures rise. In this limit we have very efficient energy transport and weak albedo feedback. At the other extreme for large λ , the net radiations converge, and the temperatures remain different by about 4°C . In this limit, the albedo sensitivity to circulation is large, but the circulation is relatively insensitive to the temperature gradients. For realistic values of the parameters, the model robustly drives the net radiation in the convective region toward that in the nonconvective region through the mechanism proposed here.

The OLR in the convective region was specified to be 190 W m^{-2} for the results shown in Fig. 10a. If lower (150 W m^{-2} ; Fig. 10b) or higher (230 W m^{-2} ; Fig. 10c) values for OLR are specified, the albedo of the clouds simply adjusts to bring the net radiation in the convective region close to that in the nonconvective region. Therefore, the feedback process will bring the net radiations close together for any reasonable value of mean OLR chosen for the convective region. This is consistent with the observed proportionality between shortwave

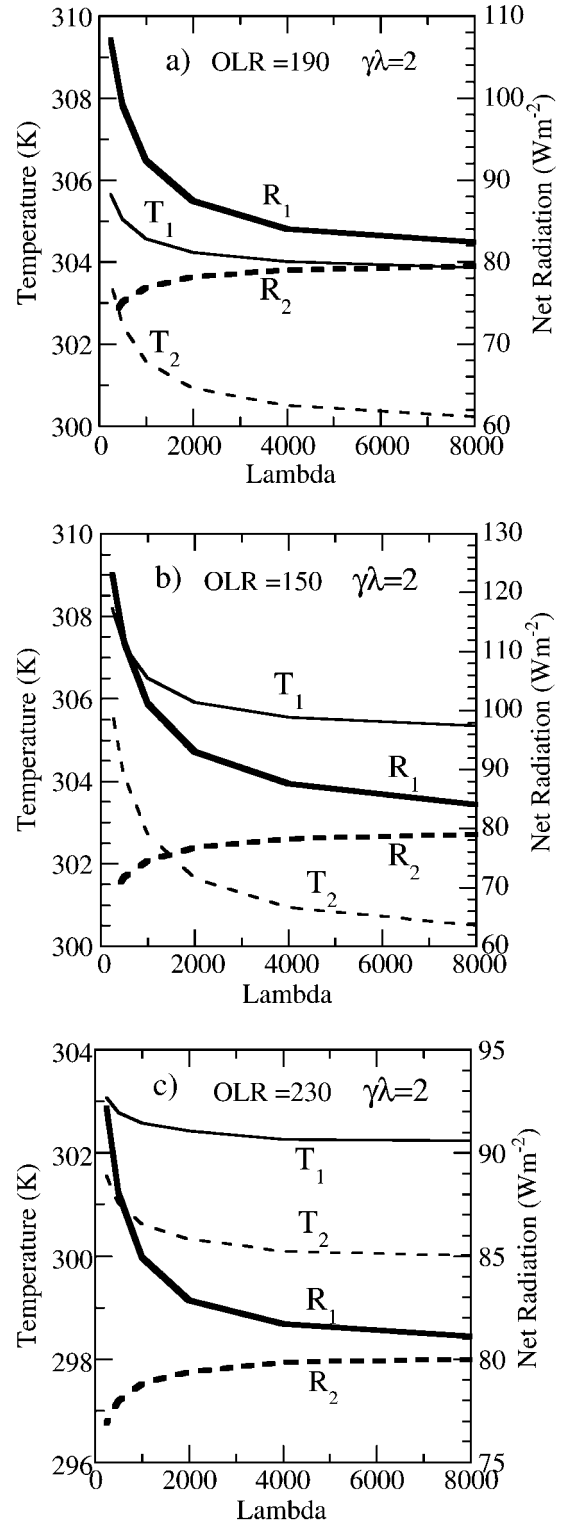


FIG. 10. SST and net radiation for convective and nonconvective regions of the two-box model for fixed sensitivity of albedo to temperature difference ($\gamma\lambda = 2$) as a function of λ . The sensitivity of cloud albedo to vertical motion for OLR in the convective region is specified to be (a) 190, (b) 150, and (c) 230 W m^{-2} .

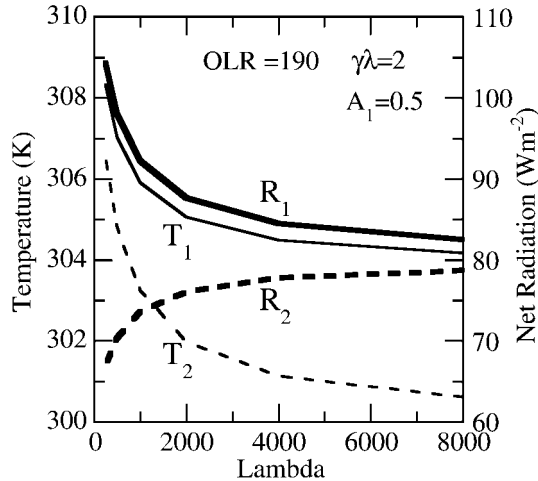


FIG. 11. Same as Fig. 10a, but for a convective area fraction of $A_1 = 0.5$.

and longwave variations in the Tropics associated with convective clouds (Hartmann and Doelling 1991).

The model behavior is not sensitive to reasonable variations in the assumption of the area occupied by the convective and nonconvective areas. If the fraction of the area occupied by convection is increased to 0.5 from 0.3, the temperatures rise a little, but the equalization of net radiation in the two regions is still efficient (cf. Fig. 11 to Fig. 10a).

We conclude that the model produces net radiations in convective and nonconvective areas that are within 10 W m^{-2} of each other for reasonable values of the model parameters. If the energy budget in the nonconvective region is close to that of clear-sky conditions, then the net cloud radiative forcing of the convective clouds is driven toward small values. This convergence of net radiation and the corresponding small net radiative effect of convective cloud are results of the sensitivity of circulation to temperature gradients in the Tropics and the sensitivity of cloud albedo to moisture convergence and mean upward motion. As transport and albedo feedback drive the SST values in the two regions closer together, the horizontal energy exchange between the two regions becomes weak, because both the mass circulation and the energy contrast between the two regions decrease.

The model employed here may also provide some insight into why some tropical convective clouds do produce net effects on the column energy balance. One can see from the Exp terms in (9) that if energy is exported from the nonconvective area or imported to the convective area, then the net radiation in the convective area will become less than in the nonconvective area. In the east Pacific ITCZ region, the net radiation shows a relative minimum and convective clouds have a net negative forcing, in contrast to the convective clouds over the west Pacific warm pool (Fig. 1). The reduction in net radiation in the east Pacific may be due

to the strong SST gradients associated with the removal of energy by the ocean circulation through the equatorial upwelling there. Another convective region with reduced net radiation is the convection over the Bay of Bengal during the summer. This may be because this cloud is influenced by the strong forcing associated with heating over the Asian landmass during the summer. In the context of the simple model, this is equivalent to adding a heat import to the convective region, which would again be consistent with the observed negative cloud radiative forcing (Fig. 1). It is also true that if the convective region interacts with a subsiding region in which the net cloud radiative forcing is negative, such as a region with extensive stratocumulus cloud decks, then the net cloud forcing in the convective region will also be driven toward negative values. This is also a possible explanation for the negative net cloud radiative forcing in the east Pacific ITCZ. Cess et al. (2001) have shown that tropical convective cloud in the Pacific developed anomalously negative cloud radiative forcing during the 1998 El Niño. We might speculate that this is because during an El Niño the convection gets more strongly organized by a strengthened Hadley circulation and a weakened Walker circulation, so that the convection across the entire Pacific is more analogous to that in the eastern Pacific in Fig. 1. This is consistent with our simple model.

8. Discussion and conclusions

It has been shown that individual deep convective cloud types observed in the Tropics have the potential to reduce strongly or to increase the net radiation in the Tropics. The visible optical depths of common convective cloud types in the upper tropical troposphere (310–180 mb) range from 1 to 60. In the near-equatorial convective Tropics over warm water, the net radiation at the top of these clouds varies from $+123$ to -16 W m^{-2} , a range of more than 100 W m^{-2} . The corresponding cloud net radiative forcings at the top of the atmosphere for these cloud types range from $+20$ to -119 W m^{-2} . This great variation in net radiative effect arises mostly from the reflectivity of the clouds, which is primarily dependent on the water and/or ice content of the clouds.

The average top-of-atmosphere net radiation in most regions of deep convection in the Tropics does not differ from the net radiation in nearby regions of suppressed convection by more than about 10 W m^{-2} . Moreover, the day-to-day variations in net radiation in convective regions have a standard deviation of only about 8 W m^{-2} . This occurs in part because variations in optically thick clouds are always accompanied by variations in optically thinner clouds and the radiative effects of the optically thick and thin clouds offset each other, if the clouds are sufficiently cold. The observed small effect of deep convective cloud complexes on the radiative energy flux at the top of the atmosphere thus is not a

property of a single uniform cloud type, but rather is a property of the ensemble of clouds that is produced by convection in the Tropics.

It is interesting and important to ask whether the top-of-atmosphere effect of deep convective cloud complexes in the Tropics is a fortuitous coincidence, as Kiehl (1994) has suggested, or may be more interesting. This property of tropical convection may provide some insight into processes in the Tropics that will be important for our interpretation of climate sensitivity. Here we have argued that the small top-of-atmosphere effect of deep convection in the Tropics is a result of a feedback process between net heating at the top of the atmosphere and the optical depth of convective clouds.

We have provided a conceptual model that suggests that the net radiation at the top of the atmosphere in convective areas is required to be near that of nearby nonconvective areas by a feedback process. The efficiency of this feedback process depends on three assumptions, which may hold true over the warmest waters of the Tropics. These assumptions are the following.

- 1) The large-scale circulation is sensitive to small variations in SST gradients.
- 2) The albedo of convective clouds is sensitive to the large-scale circulation.
- 3) Horizontal energy transport between convective and adjacent nonconvective regions is relatively small.

If the first two of these assumptions are forcefully applied, then the third tends to follow automatically and is less important. Both the circulation and the strong albedo feedback tend to drive the SSTs in the two regions toward the same value. When the temperatures are similar the energy transport must be small. The first two assumptions are coupled in the sense that the large-scale circulations are synergistic with deep convection in the Tropics. The circulation tends to be sensitive to SST gradients because of weak rotation but also because convection itself is sensitive to SST. Tropical convection tends to occur over the warmest SST, and convective intensity both drives and is favored by low-level moisture convergence and large-scale ascent. Although these arguments are posed in terms of synoptic-scale variations, the adjustment of the cloud ensemble to give small net radiative forcing must occur on the mesoscale, on timescales on the order of a day or less, because these are the time- and space scales on which tropical convective clouds evolve. Cloud structure is influenced by the mean conditions of atmospheric temperature, humidity, and SST within which the clouds play out their life cycles, and these mean conditions evolve on longer timescales.

With these feedbacks incorporated, a simple model shows that the net radiation in convective regions approaches that in adjacent nonconvective regions almost independently of the mean cloud-top temperature assumed for the convective clouds. If the nonconvective regions with which the convection interacts have small

cloud radiative forcing, then the cloud radiative forcing in the convective region must also be small. We have verified that the cloud radiative forcing in regions of suppressed convection in the deep Tropics is small even when the abundance of low clouds is substantial. These conclusions follow if the convective and nonconvective areas are nearly in equilibrium with each other. If the circulation is forced by significant ocean heat transport, as in the east Pacific, or by strong dynamical forcing associated with land-sea contrasts, as in the Bay of Bengal area, then the net cloud radiative forcing in the convective regions can be significantly negative (e.g., Fig. 1). The net radiative effect of tropical convective clouds is thus dependent on the nature of the large-scale circulation within which they are embedded, and may respond to circulation anomalies associated with El Niño, for example.

The implications of this feedback process for the sensitivity of tropical climate need to be explored more fully. Many climate models are now being introduced that include predicted rather than diagnostic cloud optical properties. The net radiative effect of tropical convective cloud in these models needs to be compared with observations to show that they produce the observed radiative neutrality of these clouds and do so for the correct reasons. The hypothesis put forward here can be tested further with models that include explicit cloud physics and incorporate the radiative effects of these clouds in a large-scale context. Single-column models (Kelly et al. 1999) and cumulus ensemble models (Lau et al. 1994) have produced tropical clouds with nearly equal longwave and shortwave cloud forcing, but it is unclear to what extent these results are sensitive to the free parameters of these models or to the mean thermodynamic conditions in these models. It is hoped that this paper will provoke interest in the small net radiative effect of tropical convective clouds and a more thorough evaluation of the mechanisms whereby this result can be achieved in models.

Acknowledgments. R. A. Houze and S. Yuter gave useful insight into the structure of tropical convective cloud systems. Two anonymous reviewers provided suggestions for improvement. This work was supported by NASA's Earth Observing System Interdisciplinary Science Program under Grant NAG5-6101. Author QF is supported in part by DOE Grant DE-FG03-00ER62931.

REFERENCES

- Barkstrom, B. R., 1984: The Earth Radiation Budget Experiment (ERBE). *Bull. Amer. Meteor. Soc.*, **65**, 1170–1185.
- , and G. L. Smith, 1986: The Earth Radiation Budget Experiment: Science and implementation. *Rev. Geophys.*, **24**, 379–390.
- , and Coauthors, 1986: First data from the Earth Radiation Budget Experiment (ERBE). *Bull. Amer. Meteor. Soc.*, **67**, 818–824.
- Brooks, D. R., E. F. Harrison, P. Minnis, and J. T. Suttles, 1986: Development of algorithms for understanding the temporal and

- spatial variability of the earth's radiation balance. *Rev. Geophys.*, **24**, 422–432.
- Cess, R. D., M. Zhang, B. A. Wielicki, D. F. Young, X.-L. Zhou, and Y. Nikitenko, 2001: The influence of the 1998 El Niño upon cloud-radiative forcing over the Pacific warm pool. *J. Climate*, **14**, 2129–2137.
- Chen, S. S., and R. A. Houze Jr., 1997: Diurnal variation and life-cycle of deep convective systems over the tropical Pacific warm pool. *Quart. J. Roy. Meteor. Soc.*, **123**, 357–388.
- , —, and B. E. Mapes, 1996: Multiscale variability of deep convection in relation to large-scale circulation in TOGA COARE. *J. Atmos. Sci.*, **53**, 1380–1409.
- Chen, T., W. B. Rossow, and Y. C. Zhang, 2000: Radiative effects of cloud-type variations. *J. Climate*, **13**, 264–286.
- Chou, M. D., 1994: Radiation budgets in the western tropical Pacific. *J. Climate*, **7**, 1958–1971.
- Collins, W. D., F. P. J. Valero, P. J. Flatau, D. Lubin, H. Grassl, and P. Pilewskie, 1996: Radiative effects of convection in the tropical Pacific. *J. Geophys. Res.*, **101**, 14 999–15 012.
- Fu, Q., 1996: An accurate parameterization of the solar radiative properties of cirrus clouds for climate models. *J. Climate*, **9**, 2058–2082.
- , and K. N. Liou, 1992: On the correlated k -distribution method for radiative transfer in nonhomogeneous atmospheres. *J. Atmos. Sci.*, **49**, 2139–2156.
- , and —, 1993: Parameterization of the radiative properties of cirrus clouds. *J. Atmos. Sci.*, **50**, 2008–2025.
- , S. K. Krueger, and K. N. Liou, 1995: Interactions of radiation and convection in simulated tropical cloud clusters. *J. Atmos. Sci.*, **52**, 1310–1328.
- , P. Yang, and W. B. Sun, 1998: An accurate parameterization of the infrared radiative properties of cirrus clouds for climate models. *J. Climate*, **11**, 2223–2237.
- Harrison, E. F., P. Minnis, B. R. Barkstrom, V. Ramanathan, R. D. Cess, and G. G. Gibson, 1990: Seasonal variation of cloud radiative forcing derived from the Earth Radiation Budget Experiment. *J. Geophys. Res.*, **95**, 18 687–18 703.
- Hartmann, D. L., 1994: *Global Physical Climatology*. Academic Press, 411 pp.
- , and D. Doelling, 1991: On the net radiative effectiveness of clouds. *J. Geophys. Res.*, **96**, 869–891.
- , and M. L. Michelsen, 1993: Large-scale effects on the regulation of tropical sea surface temperature. *J. Climate*, **6**, 2049–2062.
- , B.-M. E. Ockert, and M. L. Michelsen, 1992: The effect of cloud type on earth's energy balance: Global analysis. *J. Climate*, **5**, 1281–1304.
- , J. R. Holton, and Q. Fu, 2001: The heat balance of the tropical tropopause, cirrus, and stratospheric dehydration. *Geophys. Res. Lett.*, **28**, 1969–1972.
- Houze, R. A., Jr., 1993: *Cloud Dynamics*. Academic Press, 576 pp.
- Johnson, R. H., T. M. Rickenbach, S. A. Rutledge, P. E. Ciesielski, and W. H. Schubert, 1999: Trimodal characteristics of tropical convection. *J. Climate*, **12**, 2397–2418.
- Kalnay, E., and Coauthors, 1996: The NCEP/NCAR 40-Year Reanalysis Project. *Bull. Amer. Meteor. Soc.*, **77**, 437–471.
- Kelly, M. A., D. A. Randall, and G. L. Stephens, 1999: A simple radiative-convective model with a hydrological cycle and interactive clouds. *Quart. J. Roy. Meteor. Soc.*, **125**, 837–869.
- Kiehl, J. T., 1994: On the observed near cancellation between long-wave and shortwave cloud forcing in tropical regions. *J. Climate*, **7**, 559–565.
- , and V. Ramanathan, 1990: Comparison of cloud forcing derived from the Earth Radiation Budget Experiment with that simulated by the NCAR Community Climate Model. *J. Geophys. Res.*, **95**, 11 679–11 698.
- Larson, K., D. L. Hartmann, and S. A. Klein, 1999: The role of clouds, water vapor, circulation, and boundary layer structure in the sensitivity of the tropical climate. *J. Climate*, **12**, 2359–2374.
- Lau, K.-M., C.-H. Sui, M.-D. Chou, and W.-K. Tao, 1994: An inquiry into the cirrus-cloud thermostat effect for tropical sea-surface temperature. *Geophys. Res. Lett.*, **21**, 1157–1160.
- Lindzen, R. S., and S. Nigam, 1987: On the role of sea surface temperature gradients in forcing low-level winds and convergence in the Tropics. *J. Atmos. Sci.*, **44**, 2418–2436.
- Liou, K.-N., 1992: *Radiation and Cloud Processes in the Atmosphere: Theory, Observation, and Modeling*. Oxford University Press, 487 pp.
- Ockert-Bell, M. E., and D. L. Hartmann, 1992: The effect of cloud type on earth's energy balance: Results for selected regions. *J. Climate*, **5**, 1157–1171.
- Ramanathan, V., and W. Collins, 1991: Thermodynamic regulation of ocean warming by cirrus clouds deduced from observations of the 1987 El Niño. *Nature*, **351**, 27–32.
- , R. D. Cess, E. F. Harrison, P. Minnis, B. R. Barkstrom, E. Ahmad, and D. Hartmann, 1989: Cloud-radiative forcing and climate: Results from the Earth Radiation Budget Experiment. *Science*, **243**, 57–63.
- Rossow, W. B., and Y. C. Zhang, 1995: Calculation of surface and top of atmosphere radiative fluxes from physical quantities based on ISCCP data sets. 2. Validation and first results. *J. Geophys. Res.*, **100**, 1167–1197.
- , and R. A. Schiffer, 1999: Advances in understanding clouds from ISCCP. *Bull. Amer. Meteor. Soc.*, **80**, 2261–2287.
- Schiffer, R. A., and W. B. Rossow, 1985: ISCCP global radiance data set: A new resource for climate research. *Bull. Amer. Meteor. Soc.*, **66**, 1498–1505.
- Schubert, S., S. Moorthi, C.-K. Park, M. Suarez, and W. Higgins, 1990: An atlas of ECMWF analyses (1980–87). NASA Tech. Memo. 100747, 258 pp.
- Tompkins, A. M., and G. C. Craig, 1999: Sensitivity of tropical convection to sea surface temperature in the absence of large-scale flow. *J. Climate*, **12**, 462–476.
- Yuter, S. E., and R. A. Houze Jr., 2000: The 1997 Pan American Climate Studies Tropical Eastern Pacific Process Study. Part I: ITCZ region. *Bull. Amer. Meteor. Soc.*, **81**, 451–481.
- Zhang, Y. C., W. B. Rossow, and A. A. Lacis, 1995: Calculation of surface and top of atmosphere radiative fluxes from physical quantities based on ISCCP data sets. 1. Method and sensitivity to input data uncertainties. *J. Geophys. Res.*, **100**, 1149–1165.